Surface Microroughness of Optical Glasses under Deterministic Microgrinding

The Center for Optics Manufacturing (COM) at the University of Rochester has made significant advances in the fabrication of precision optical components using deterministic microgrinding with rigid, computer-controlled machining centers and high-speed tool spindles. In deterministic microgrinding, the infeed rate of the microgrinding tool across the optical workpiece is optimized and controlled. This leads to precise knowledge of the amount of removed material when microgrinding optical glasses. This method has been applied to manufacturing convex and concave spherical surfaces with radii 5 mm to ∞ (i.e., planar), and work diameters from 10 to 150 mm have successfully been formed.[1–5] Aspherical surfaces have also been manufactured. After less than 5 min of deterministic microgrinding, the resulting specular surfaces have typical rms microroughness of less than 20 nm, 1 μm of subsurface damage, and a surface figure better than 1/2 wave peak to valley.[6] Typical infeed rates are 6 to 10 μm/min with 2- to 4-μm bound-abrasive diamond tools.

An overview of the mechanics and materials used in deterministic microgrinding has been presented previously at the structure/component level, involving length scales from 1 m to 1 mm, and at the process/materials level (1 mm to 1 nm).[7] The various chemomechanical interactions between abrasives and the glass surface can be categorized in terms of various length scales describing the response of the material to chemomechanical inputs.[8]

The bound-abrasive tools used in this work consist of single-crystal or polycrystal diamonds embedded in a bronze-type ring, typically 50 mm in diameter. The hardness of the tool is controlled using various amounts of binder material and by varying the processing conditions. Typically, several tools with decreasing abrasive sizes are used to create the desired surface profile and finish. Each tool is used to remove the damaged layer resulting from the previous tool and to further reduce the surface microroughness. The size of the diamond abrasives vary from about 100 μm down to 2 to 4 μm. Typical tool rotation rates for deterministic microgrinding of optical glasses range from 5,000 to 30,000 rpm, while the work rotation rates are from 50 to 300 rpm. Aqueous coolants are used to facilitate the mechanical and chemical actions of the bound-abrasive tools. The tool microstructure and performance have been discussed by Khodakov and Glukhov,[9] and the tool mechanical properties and microstructure, primarily porosity, have been investigated by Funkenbusch and co-workers at the University of Rochester.[10,11]

It is well known that microgrinding may entail either ductile or brittle material-removal mechanisms.[12–14] Either mode may become dominant depending upon mechanical factors, such as depth of cut,[15] or chemomechanical factors, such as coolant chemistry,[16,17] or abrasive size.[16–18] The brittle-to-ductile transition occurs under loose-abrasive microgrinding conditions of planar surfaces,[16,17] bound-abrasive microgrinding in plunge mode on planar surfaces[15,18] or aspheres,[14] and in single-point diamond turning of planar surfaces.[19]

At sufficiently low depths of cut, material removal occurs by plastic scratching. This mode is known as ductile or shear-mode grinding[20,21] and is characterized by low surface microroughness and subsurface damage, low material-removal rates, and high residual surface stresses.[17] In some cases the latter approaches the flow stress of glass in a thin surface layer.[22]

When the depth of cut is high or the abrasive size large, brittle material removal occurs and is characterized by high material-removal rates (proportional to the abrasive size[20,21,24–26]), considerably higher surface microroughness (proportional to the abrasive size[20,21,23]), a subsurface damage depth (generally proportional to the microroughness[27–30]), and lower levels of residual surface stress.[25–28]

One important aspect of deterministic microgrinding is that different glasses, microground under the same operating conditions, produce different amounts of surface microroughness and subsurface damage. This is not surprising since the mechanical properties of the glasses clearly affect their response to deterministic microgrinding. It has been shown that the mechanism for fine grinding using bound diamond tools de-

pends on the properties of the glass, as well as on the acidity of the grinding fluid, and the chemical and mechanical properties of the abrasive bond.[29] However, those studies did not actually correlate the observed grinding response with specific glass properties. That correlation had been performed using a brittleness index to characterize the response of glasses and ceramics under loose-abrasive grinding conditions.

In loose-abrasive grinding, surface roughness correlates with glass hardness,[31] whereas in deterministic microgrinding (where the infeed rate is specified), the elastic, plastic, and fracture properties of the work must all be used to predict microroughness. Under conditions where the nominal pressure is constant rather than the infeed rate, the average surface peak-to-valley microroughness (measured with a mechanical profilometer) was in the range of 2 to 20 μm for removal rates of 0.2 to 2.0 μm s^{-1}.[31] The abrasives, SiC or Al$_2$O$_3$, had sizes 150 μm or 22 μm, respectively. It was also shown that the surface microroughness was proportional to $E^{1/2}/H_v$, and the linear removal rate (μm s^{-1}) was proportional to $E^{5/4}/(K_c H_v^2)$, with E denoting the Young's modulus, K_c the fracture toughness, and H_v the Vickers microhardness. It was expected that the microroughness was proportional, if not identical, to the depth of the plastic zone on the glass surface, which, in turn, is determined by E and H_v when the surface is indented by a force of constant magnitude. It will be shown here that this model cannot be applied to deterministic microgrinding conditions where the infeed rate, rather than the nominal pressure, is specified.

To fully understand the interaction between the grinding tool and the optical surface in deterministic microgrinding, one must consider the effects of individual abrasive grains (or groups of grains) on the material-removal rate.[32] Such effects are governed by the chemomechanical properties of the glass, the bond matrix, and the abrasive grain, as well as by the process parameters, such as tool rotation rate and infeed rate. These effects are measured in terms of the resulting quality of the ground surface determined, for example, by the surface microroughness and subsurface damage.

To examine the correlation between mechanical properties and surface quality, a large set of glasses were ground under nominally identical operating conditions (i.e., tool and work rotation rates, infeed rate, tool diameter, and diamond concentration). In these microgrinding experiments, a sufficient amount of glass was removed so as to produce an optimal surface roughness. The mechanical properties of the various glasses spanned a relatively wide range and are summarized for some representative optical glasses. The correlation of surface microroughness to these glass mechanical properties for deterministic microgrinding is shown.

Experimental Procedure

1. Glass Properties

The chemical compositions of the glasses tested are shown in Table 66.I. The majority of the fused silica samples were Corning C7940.

Vickers hardness was measured by microindentation, with load application times of 15 s. The load was typically in the range of 2 to 1,000 gf (about 0.02–10 N). For each load, five indentations were made, and for each indentation the impression diagonals were measured three times. All glasses were measured in air. Figure 66.41 shows the dependence of the measured Vickers hardness on the applied load for some representative glasses, among which are fused silica, crown borosilicate, and flint glasses. Note that the flint glasses are relatively soft compared to the crown glasses and fused silica.

Table 66.I: The chemical compositions of the tested glasses (mol %). Both the Schott and Hoya glass designations are given. The majority of the fused silica samples were Corning C7940.

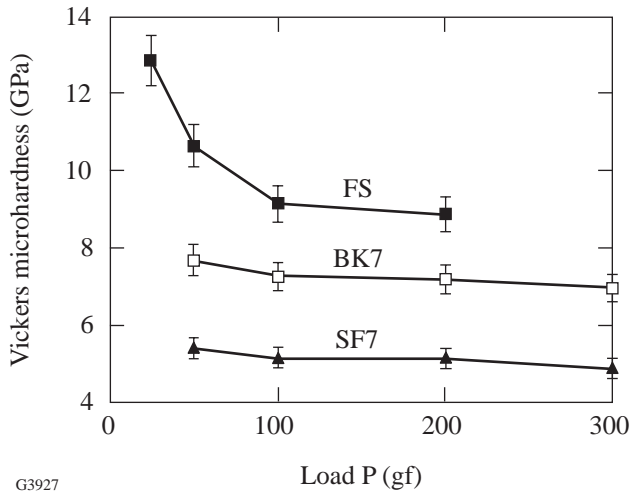| Glass (Schott)	Glass (Hoya)	SiO$_2$	B$_2$O$_3$	Al$_2$O$_3$	Na$_2$O	K$_2$O	CaO	BaO	PbO	Sb$_2$O$_3$	As$_2$O$_3$
Fused silica		100	–	–	–	–	–	–	–	–	–
F7	F7	44.75	–	–	2.4	5.7	–	–	46.85	–	0.3
SF7	FD7	33	–	–	–	5	–	–	62	–	–
SK7	BaCD7	39	15	5	–	–	–	41	–	–	–
BK7	BSC7	68.9	10.1	–	8.8	8.4	–	2.8	–	–	1
K7	C7	74	–	–	9	11	6	–	–	–	–
KzF6	SbF6	54	17.1	1.1	0.3	6	–	–	–	21	0.5

G3927

Figure 66.41
Load dependence of the Vickers microhardness for some optical glasses. FS is fused silica, BK7 is a crown borosilicate, and SF7 is a flint silicate glass. The hardness was measured at loads of 2, 5, 10, 25, 50, 100, 200, 500, and 1000 gf.

It is clear that the measured hardness increases at lower loads. This is a manifestation of the indentation size effect (ISE),[33] which can be described as

$$H_v = H_\infty \left(1 + \frac{D_0}{D}\right), \qquad (1)$$

where H_v is the measured hardness, H_∞ is the hardness at large loads, D_0 is a parameter describing the ISE, and D is the indentation diagonal. These parameters were extracted by plotting the measured H_v versus $(1/D)$. Table 66.II summarizes the curve-fitting results, where D_{min} and D_{max} are the smallest and largest indentation diagonals used in the fitting.

Figure 66.42 compares the measured Vickers hardness in the present work and in the work of Izumitani[34] to the published Knoop hardness. The two lines are parallel to each other. The offset at small Knoop hardness may be due to the fact that the junction offset in the Vickers indenter used (estimated at about 1 μm from atomic force microscopy of indentation shapes on soft materials such as ZnSe) may have been different from the one used in the work of Izumitani.[34]
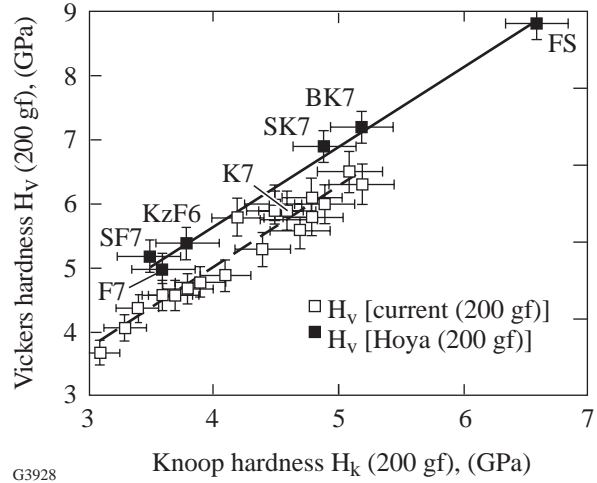

G3928

Figure 66.42
Comparison of measured Vickers microhardness with published values of the Knoop hardness from the Hoya and Schott glass catalogs. The open squares are the Vickers data from Izumitani.[34]

For fracture toughness measurements, the length c of cracks emanating from the indentation corners was measured. Typical data are shown in Fig. 66.43. For the glasses F7, SF7, and BK7, no cracks were observed for the three lowest loads used (2, 5, or 10 gf), but cracks were observed at 25 gf. For

Table 66.II: Parameters H_∞ and D_0 describing the indentation size effect (ISE) for the optical glasses used. The table shows also the range of indentation diagonal and Vickers hardness measured. The smaller diagonal corresponds to the higher hardness.

Glass	D_{min}–D_{max} (μm)	H_{max}–H_{min} (GPa)	H_∞ (GPa)	D_0 (μm)	R
BK7	11–51	7.7–6.9	6.7±0.1	1.6±0.2	0.975
SF7	13–61	5.4-4.8	4.7±0.1	1.9±0.3	0.945
F7	27–65	4.9–4.4	4.1±0.1	5.4±0.7	0.965
SK7	15–54	7.6–6.3	5.6±0.1	5.6±0.4	0.990
K7	11–57	7.8-5.6	4.7±0.1	6.8±0.5	0.988
KzF6	11–59	6.8–5.3	4.6±0.1	5.3±0.6	0.972
FS	6–21	12–8.8	6.9±0.3	5.1±0.6	0.994

K7, the loads for cracking were in excess of 50 gf, with no cracks for 25 gf or lower. For KzF6, the corresponding loads were 200 gf and 100 gf. These cracking thresholds indicate that KzF6 has the highest threshold load for cracking (the threshold being in the range 100 to 200 gf), K7 had the second highest threshold (between 25 and 50 gf), and the other glasses had threshold loads of about 25 gf.
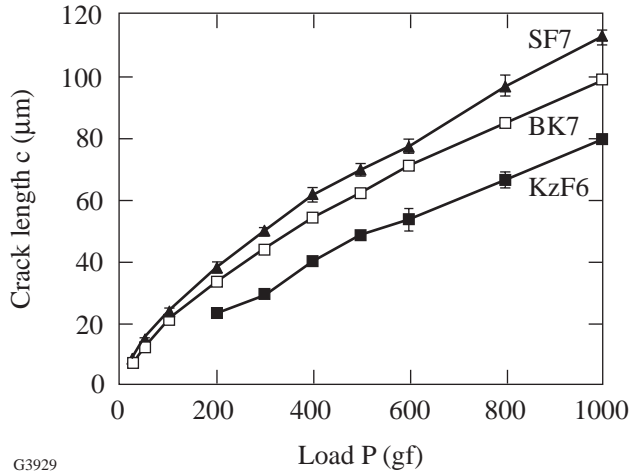

G3929

Figure 66.43
The dependence of the crack length c on the load P for typical optical glasses.

Two separate crack systems can arise from a Vickers micro-indentation.[35,36] Most ceramics with low fracture toughness exhibit half-penny cracks, also known as radial cracks. Brittle materials with small crack lengths, or, equivalently, materials with high fracture toughness, exhibit Palmqvist cracking. We observe that the measured total crack size $2c$ is the distance between crack tips on the surface trace of the radial crack.

The dependence of the measured crack length c on the applied load P exhibited both effects. The dependence $P \sim c^{3/2}$, which is usually assumed, was not exhibited; that relationship is based on the assumption of point loading a penny-shaped crack and is only valid when the crack size $c \gg$ indentation half-size $D/2$. In our measurements on glasses and crystals (such as sapphire, KDP, and LiNbO$_3$), we had $c/(D/2)$ in the range 2.5 to 5.5. Indeed, the relation $P \sim c^{3/2}$ is obeyed only at large crack sizes, whereas at smaller crack sizes $P \sim c$. Thus, we used (see also Table 66.III)

$$c = \alpha\, P^{2/3} + \beta\, P. \qquad (2)$$

Once the dependence of the crack size c on P has been measured, the fracture toughness K_c, a material property, can be calculated in a variety of ways.[37–44]

Table 66.III: Coefficients in correlating the measured crack size c to the applied load P according to the relation $c = \alpha\, P^{2/3} + \beta\, P$ for the six glasses tested.

Glass	α (μm N$^{-2/3}$)	β (μm N^{-1})	R
SF7	23.2±0.8	0.5±0.4	0.99965
F7	21.3±0.8	1.1±0.4	0.99954
BK7	21.2±0.5	0.06±0.25	0.99982
SK7	19.3±1	0.8±0.6	0.99912
K7	18.4±1	0.3±0.5	0.9989
KzF6	11.4±1.2	2.6±0.6	0.9982

The approaches of Niihara *et al.*[42] and Shetty *et al.*[43] assume surface cracks are Palmqvist type, whereas others assume the cracks to be fully developed radial cracks. Evans[38] used dimensional analysis and curve fitting over a range of $c/(D/2)$ from 1.5 to 7 and for many ceramic materials (B$_4$C, SiC, Si$_3$N$_4$, WC/Co, ZnS, ZnSe, PSZ ZrO$_2$). This model should be applicable to both Palmqvist and radial cracks, according to the following:

$$K_c = H\sqrt{D/2}\left(\frac{E}{H}\right)^{0.4} 10^{f(x)}, \qquad x = \log_{10}\left(\frac{c}{D/2}\right)$$

$$f(x) = -1.59 - 0.34\, x - 2.02\, x^2 \qquad (3)$$

$$+ 11.23\, x^3 - 24.97\, x^4 + 16.32\, x^5,$$

where K_c is the fracture toughness, H is the hardness, D is the indentation diagonal, E is the Young's modulus, and c is the half-crack size. Lankford[41] included Al$_2$O$_3$, soda-lime silicate glass, and NaCl to the materials analyzed by Evans.[38] Anstis *et al.*[40] examined various glasses (glass-ceramic, soda-lime, aluminosilicate, lead alkali), polycrystal Al$_2$O$_3$ and sapphire, Si$_3$N$_4$, SiC, Ca-PSZ ZrO$_2$, Si, and SiC/Co. In the present work, $c/(D/2)$ ranges from about 2 to 3.8 and, therefore, should be described by Eqs. (3). For each indentation load P, diagonal D, and crack size c, we used the measured value of the Vickers hardness corresponding to that specific load. All models considered yielded the same relative ranking of the fracture toughness of these glasses.

Microindentation fracture toughness tests in toughened ZrO$_2$ (Ce-TZP), as well as bulk fracture toughness testing, were used to study this problem (bulk testing with the double

cantilever beam technique gave $K_c = 10.2$ MPa $m^{1/2}$).[45] By comparing the bulk test results with the microindentation test results, it was concluded that the analysis according to Palmqvist cracking was not very successful, that the Lankford[41] and Niihara[42] analyses overestimated the fracture toughness, and that the Evans[38] and Anstis *et al.*[40] approaches gave results most consistent with the bulk tests.

The extracted fracture toughness in Table 66.IV, which also includes other mechanical properties of glass, is summarized. The values in the table are averages over all crack lengths measured. The indicated errors correspond to the standard deviation over that range of crack lengths. Figure 66.44 shows the relation of the measured fracture toughness with the Knoop hardness (measured with a load of 200 gf), taken from the Schott Glass catalog.[46] It is seen that, in general, the silicate flint glasses (SF6, SF56, SF7, F7) are soft and brittle, whereas the silicate crown glasses (K7, BK7, SK7, fused silica) are harder and tougher. Note, however, that the antimony flint glass KzF6 has an exceptionally high toughness, as does the lanthanum borate glass LaK10. The effects of mechanical properties on surface microroughness will be discussed.

A literature survey was performed to confirm that the fracture toughness of some materials tested by microindentation

has also been tested by other methods. For the borosilicate crown glass BK7, Wiederhorn *et al.*[50] measured a fracture toughness of 0.85 ± 0.05 MPa $m^{1/2}$ at room temperature using double cantilever specimens. The fracture toughness of BK7 has been measured also in the range of 0.84 to 0.86 MPa $m^{1/2}$
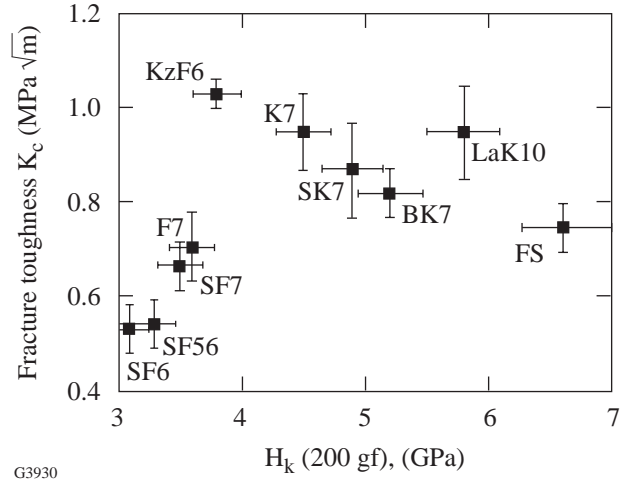

Figure 66.44
The correlation with Knoop hardness (from the Schott catalog[46]) of the measured microindentation fracture toughness K_c, extracted from $c(P)$ with the model of Evans.[38]

Table 66.IV: Mechanical properties of representative optical glasses. The microindentation data compare the extracted fracture toughness K_c (units of MPa $m^{1/2}$) based on the data of Cumbo,[47,48] Izumitani,[34] and the current work. All data have been reduced using the model of Evans.[38] Cumbo[47] used a load of 500 gf in air. Cumbo[48] used indenting loads of 50, 100, and 200 gf in anhydrous methanol. Izumitani[34] used 200 gf in air. The bulk measurements of SF6 used the Barker short-rod technique.[49] The bulk measurements of BK7 and fused silica were performed using the double cantilever method (DCB),[50] single-edge-notch, 3-pt. bending (SENB),[51] or strength method using a Knoop indent.[31]

	SF6	SF7	F7	BK7	SK7	K7	KzF6	FS
ρ (g cm^{-3})	5.18	3.80	3.62	2.51	3.51	2.53	2.54	2.20
T_g (°C)	426	448	437	557	643	513	444	1090
E (GPa)	56	56	55	81	84	69	52	73
H_k (200 gf) (GPa)	3.1	3.5	3.6	5.2	4.9	4.5	3.8	6.6
Cumbo[47] K_c	–	0.63±0.03	0.69±0.04	0.86±0.04	0.86±0.04	0.91±0.05	–	–
Cumbo[48] K_c	0.54±0.04	–	0.68±0.04	0.86±0.08	–	–	–	–
Izumitani[34] K_c	0.54	–	–	0.85	–	–	–	–
This work K_c	–	0.67±0.05	0.71±0.07	0.82±0.05	0.87±0.10	0.95±0.08	1.03±0.03	–
Bulk K_{Ic}	0.54	–	–	0.85±0.05	–	–	–	0.75±0.05

using the double cantilever method and three-point bending of edge-cracked specimens.[51] More recently, Buijs and Korpel-Van Houten[31] used a three-point bend test and Knoop indentation cracks to find 0.83±0.08 MPa $m^{1/2}$.

Our current measurements (see Table 66.IV) and the use of the Evans model[38] for the determination of fracture toughness gave 0.82±0.05 MPa $m^{1/2}$. Cumbo's microindentation measurements,[48] with loads in the range of 50 to 200 gf, when analyzed with the Evans model, gave a fracture toughness of BK7 0.86±0.08 MPa $m^{1/2}$ in anhydrous methanol. Cumbo's[47] older measurements in air, with a load of 500 gf, gave 0.86±0.04 MPa $m^{1/2}$ when analyzed with the Evans model.

We also note that Izumitani[34] used Vickers microindentation at a load of 200 gf and measured a crack size of $c = 34.5$ μm for BK7 in air. Although no measurement errors were reported, when these measurements are reduced with the Evans model, the microindentation fracture toughness for BK7 is extracted as 0.85 MPa $m^{1/2}$.

We conclude that microindentation fracture measurements in BK7 glass, when reduced according to the model by Evans,[38] give close agreement with the fracture toughness as measured by various bulk methods. Various microindentation measurements are also self-consistent in that all predict the same microindentation fracture toughness for BK7.

For the flint glass SF6, the bulk fracture toughness has been measured with Barker's short-rod technique in the work of Androsov et al.,[49] who used the Russian designation TF10 for that glass. In the short-rod technique, the fracture toughness was reported as 0.54 MPa $m^{1/2}$. More recently, Buijs and Korpel-Van Houten[31] used a three-point bend test and Knoop indentation cracks to find 0.54±0.05 MPa $m^{1/2}$.

Although we have not measured SF6 in this work, Cumbo did so in his Ph.D. thesis[48] using Vickers microindentation with loads of 50, 100, and 200 gf. We used the model by Evans[38] to reduce the microindentation measurements by Cumbo. The fracture toughness of SF6 is found to be 0.54±0.04 MPa $m^{1/2}$, in excellent agreement with the bulk measurement of Androsov et al.[51]

We also note that Izumitani, in a Hoya technical report,[34] used Vickers microindentation at a load of 200 gf and measured a crack size $c = 49.2$ μm. When these measurements are reduced with the Evans model,[38] the microindentation fracture toughness is extracted as 0.54 MPa $m^{1/2}$. Again, it is concluded

that microindentation fracture toughness measurements of SF6 are self-consistent, and they agree well with independent measurements of the bulk fracture toughness.

For fused silica, microindentation analysis overestimates the actual fracture toughness because fused silica is known to densify under compressive loads,[52,53] rather than flow by shear. Densification is facilitated by shear stresses.[54] Consequences of densification for optics manufacturing applications, such as polishing or grinding, are discussed by Lambropoulos et al.,[55] who also listed, from the literature, different glass types that are known to densify.

The bulk fracture toughness of fused silica has been measured by various techniques. For example, Wiederhorn[56] has measured 0.75 MPa $m^{1/2}$ with the double cantilever method, in agreement with the measurements by Wiederhorn et al.;[50] Barker[57] used a short-rod technique to measure 0.735±0.01 MPa $m^{1/2}$. The NBS work[51] used both double cantilever and edge cracked three-point bending techniques and measured 0.74 to 0.75±0.03 MPa $m^{1/2}$. Buijs and Korpel-Van Houten[31] used a three-point bend test and Knoop indentation cracks to find 0.70±0.07 MPa $m^{1/2}$. In the correlations to follow, we will therefore use 0.75 MPa $m^{1/2}$ for the fracture toughness of fused silica.

For other optical glasses, Izumitani in a Hoya technical report[34] used Vickers microindentation to measure the indentation diagonal and crack size for a large number of optical glasses, although these measurements were not converted to a fracture toughness. In that work, the crack length is defined as that portion of the crack trace extending beyond the end of the indentation diagonal (see also Izumitani,[13] p. 105, Fig. 4.32). For some glasses, the crack size was reported but not the indentation diagonal (see Izumitani,[13] p. 105, Fig. 4.31). Since these measurements are useful in correlating the glass mechanical properties with the surface quality, as described in the following sections, the model of Evans[38] was used to extract the fracture toughness of these glasses from the Izumitani measurements. The results are summarized in Table 66.V.

Microindentation is a convenient testing method for measuring the mechanical properties of glasses. For optical glasses not exhibiting densification, the fracture toughness from microindentation (determined by the measurement of the crack size at a fixed load) is in good agreement with bulk measurements. For densifying glasses, such as fused silica, microindentation overestimates the fracture toughness as measured by bulk methods.

Table 66.V: The extracted fracture toughness, according to the microindentation model by Evans,[38] for the optical glasses tested by Izumitani.[34] The data for the Young's moduli and Knoop hardness H_k (at 200 gf) are from the Schott Optical Glass catalog.[46] Parentheses ( ) in the E or H_k values show that the property was estimated from those of neighboring glasses. The Vickers hardness is extracted from the measurements of Izumitani[34] with a load of 200 gf. The ( ) in the H_v value indicate that the Vickers hardness was estimated from the correlation of H_v and H_k, similar to the one shown in Fig. 66.43, using the data from Izumitani.[34] The ( ) in the K_c entry denote that the estimated H_v for that glass was used. The bulk measurements of K_c for SF1 and UBK7 are from Wiederhorn and Roberts;[51] for F2 from Buijs and Korpel-Van Houten;[31] for SF6 from Buijs and Korpel-Van Houten[31] and Androsov.[49] The uniaxial yield stress σ_Y was estimated using the model of Hill[58] (see Appendix).

Glass (Schott)	E (GPa)	H_k (GPa)	H_v (GPa)	K_c (MPa $\sqrt{m}$)	K_c (MPa $\sqrt{m}$) (bulk)	σ_Y (GPa)
F2	58	3.7	4.6	0.61	0.55±0.06	1.9
F4	55	3.6	4.6	0.65		2.0
F5	58	3.8	4.7	0.63		2.0
SF1	56	3.4	(4.3)	–	0.63±0.09	2.1
SF4	56	3.3	4.1	0.55		1.7
SF5	56	3.4	4.4	0.57		1.8
SF6	56	3.1	3.7	0.54	0.54	1.4
SK3	83	4.8	6.1	0.77		2.5
SK11	79	5.1	6.5	0.78		2.8
SK15	84	4.5	6.0	0.79		2.4
SK16	89	4.9	6.0	0.78		2.3
BK1	74	4.8	5.8	0.82		2.5
UBK7	81	5.0	(6.2)	–	0.89±0.01	2.6
K3	71	4.7	5.6	0.79		2.4
K9	(67)	(4.4)	5.3	0.76		2.3
KF4	(66)	(4.1)	4.9	0.76		2.0
LF6	60	3.9	4.8	0.72		2.0
LaF2	93	4.8	(6.0)	(0.94)		2.3
LaF3	95	5.1	(6.3)	(0.93)		2.4
LaK10	111	5.8	(7.2)	(0.95)		2.7
LaK11	90	5.2	(6.5)	(0.83)		2.5
BaK2	71	4.5	(5.6)	(0.72)		2.4
BaF3	64	4.2	(5.2)	(0.67)		2.2
BaF10	78	(4.8)	5.8	0.67		2.3
BaSF2	66	4.1	(5.1)	(0.44)		2.1
BaSF8	74	(4.2)	5.8	0.67		2.1
SSK1	79	4.5	5.9	0.75		2.4
SSK5	(79)	(4.6)	5.9	0.70		2.4

2. Deterministic Microgrinding

All samples subjected to deterministic microgrinding were nominally prepared under the same conditions. Typically, the final 2- to 4-μm tool was run at 15,000 rpm, with a work speed of 180 rpm, an infeed rate of 6 μm min^{-1}, a total material removal of 12 μm, and a dwell time after infeed of 15 s. Occasionally, these parameters were altered slightly to achieve the least possible roughness for a given glass. The most common cutting parameter changed was the total amount of glass removed with the 2- to 4-μm tool. This could be as low as 5 μm for some materials, depending on the residual damage depth from the previous tool. Occasionally, tool rpm was reduced or dwell time was increased. Tools were trued and dressed before each microgrinding cut.

3. Tool Property Characterization

Various-hardness tools were used[59] but all tools had a 75 concentration of 2- to 4-μm diamonds (18.8 vol %) and a Young's modulus of 100 to 120 GPa. The aqueous coolant used is commercially available as Challenge 300 HT and has pH = 9.5.

Bond properties for bound-abrasive tools are generally described in terms of the bond "hardness." The tools used in this study were bronze bonds with bond hardnesses designated as L (softer), N (medium), and T (harder). Bond hardness is an alphabetical scale with the hardness increasing for designators from A (soft) to Z (hard). Unfortunately, there is no universal scale for this designation, nor even good agreement on what specific property constitutes a bond's hardness. We have, therefore, used simple mechanical tests to characterize bond properties: the ultrasonic wave speed and Vickers microhardness.

When an ultrasonic wave traverses a solid, its speed (v) is determined by the modulus (M) and density (ρ) of the material in accordance with

$$v = \sqrt{\frac{M}{\rho}}. \tag{4}$$

The particular modulus M measured (Young's modulus, shear modulus, etc.) depends on the type of wave and some geometrical details of the testing procedure. For an isotropic material with only two independent elastic constants, measurement of both P-wave (compression) and S-wave (shear) speeds allows both constants to be determined. Therefore, if the wave speed and the density of a tool material are determined, a quantitative measure of its elastic stiffness can be obtained.

In the current experiments, the density could not be measured nondestructively since the bond material was permanently fused to the stainless steel rings during the fabrication process. Therefore, the wave speeds were used as indicators of elastic stiffness, with the assumption that the tool densities are all similar. This is reasonable since the bonds were all bronze based and had identical diamond concentrations. The relatively small differences in the observed wave speeds (see Fig. 66.45) are therefore indicative of relatively small differences in elastic stiffness among the different designation tools.
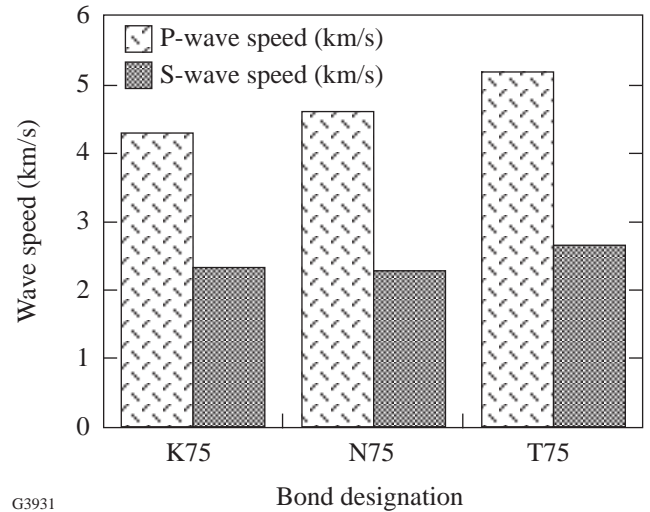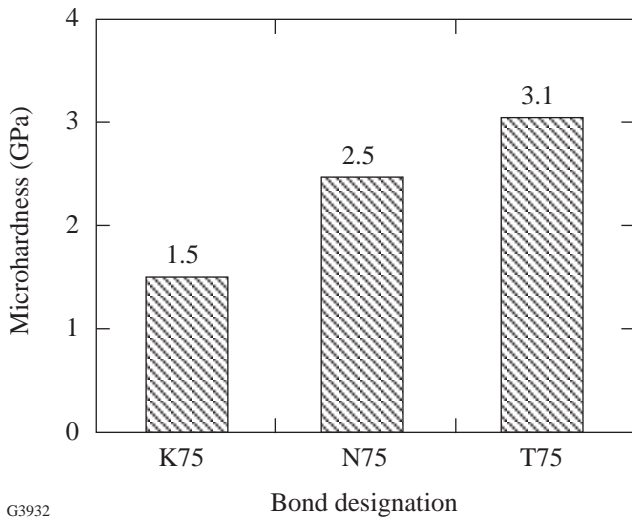

Figure 66.45
Measured ultrasonic wave speeds for different bond-hardness designations.

Vickers microhardness was also measured on the tools, using a 200-gf load. A much stronger trend in the data is obtained in this case (Fig. 66.46), with the T bond microhardness being approximately double that of a K bond. The L bond was not measured but should be between that of the K and N bonds. Considerable variation can occur among individual microhardness test results as a consequence of the locally inhomogeneous nature of the bond. The reported values are therefore averages of at least five separate indentations. Standard deviations for these measurements were of the order of 0.1 to 0.2 GPa.

4. Surface Roughness (SR) and Subsurface Damage (SSD)

The surface microroughness was interferometrically measured with a Zygo Maxim (MX) or Zygo New View 100 (NV) interferometer. The Zygo New View 100 is a three-dimensional imaging surface-structure analyzer. It uses coherence-scanning white-light interferometry for noncontact imaging and measurement of surface microstructure and topography.
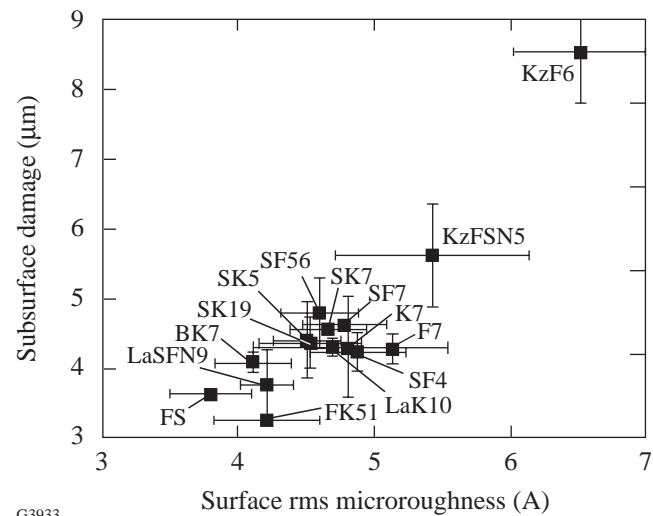
Figure 66.46
Measured Vickers microhardness for different bond-hardness designations.

The Zygo Maxim uses the same interferometric principles but has a laser as a light source and does not scan vertically. Because of these differences, this device cannot measure absolute surface roughness on components with defects exceeding about 0.5 μm. The rms surface roughness values reported for microground surfaces are substantially lower than the actual roughness, but are qualitatively reliable.

For each glass, 12 to 15 optical surfaces, prepared under the same microgrinding conditions, were used for the surface-roughness determination with the Zygo Maxim interferometer. The roughness of a smaller set of glasses (nine samples per glass type) was also measured with the New View 100 interferometer.

Following microgrinding, the subsurface damage (SSD) was determined by first etching the samples in HF for 30 s to reveal the structure below the surface. Damage depth is measured by a dimpling technique, described by Lindquist et al.,[60] in which a steel ball of 23.81-mm radius is used with an abrasive to polish a dimple in the etched region. SSD is extracted by optically measuring the inner and outer radii containing the damaged layer. For a given steel ball radius, these measurements provide the depth that damage extends below the surface. Zhou et al.[61] have shown that optical measurement of SSD is in good agreement with SEM measurements for a variety of etching solutions and durations. The subsurface damage was measured in two different samples prepared under nominally identical microgrinding conditions.

The measured surface microroughness (from the Maxim interferometer) is plotted in Fig. 66.47 versus the subsurface damage measured by dimpling. It is seen that, generally, the subsurface damage increases with surface roughness. Similar observations were originally made by Aleinikov[27] for loose abrasive grinding of glasses and ceramics. Aleinikov used a profilograph to measure peak-to-valley surface roughness in the 35- to 65-μm range for glasses, and subsurface damage in the 150- to 260-μm range. The abrasive used was SiC of about 100 to 150 μm in size. The ratio of roughness to subsurface damage was found to be 4 to 4.2 for the tested optical glasses.

Figure 66.47
Comparison of the measured subsurface damage and the surface roughness (measured with the Zygo Maxim interferometer). For each glass, about 12 different samples were used for the roughness and two samples for the subsurface damage measurements.
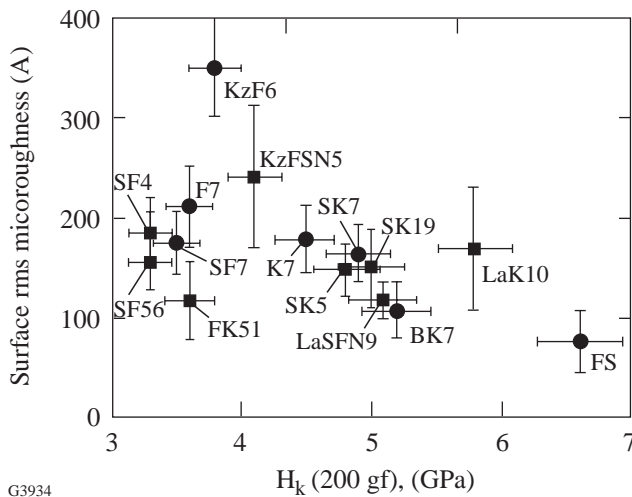
Edwards and Hed[30] investigated the relationship between surface roughness and subsurface-damage depth for bound-diamond-abrasive tools (diamond size 60 to 220 μm), identifying both fracture and plastic scratching as the material-removal mechanisms. This is in contrast to the work on loose-abrasive lapping,[27] where material removal occurred only by fracture. For BK7 and zerodur, Edwards and Hed[30] found peak-to-valley surface roughness (measured with a stylus profiler) of 1.2 to 8 μm and subsurface damage depth (measured with a taper polishing method) in the range 15 to 42 μm. For conditions with fracture as the principal material-removal mechanism, they found the ratio of subsurface-damage depth to peak-to-valley surface roughness as 6.4±1.3.

That work also examined the review work of Khodakov *et al.*[28] (unspecified glasses and grinding conditions) on bound diamond tools and estimated a ratio of subsurface damage to roughness of 5.5±1.1 for diamond particles 6.5 to 40 μm in size.

Correlations

In this section we discuss some correlations between the measured surface rms microroughness (SR) and the material properties of the glasses tested. The surface roughness data are those obtained from components ground with the N75 (medium bond hardness) tool with 2- to 4-μm diamonds and measured with the Maxim interferometer. For the correlations we use Knoop hardness, as it is conveniently tabulated in manufacturers' product catalogs.[46]

Figure 66.48 shows the correlation of measured surface roughness (SR) with the Knoop hardness H_k (measured at 200 gf) from the Schott Glass catalog.[46] This figure shows that, with the hardness as the correlating mechanical property, surface roughness increases with hardness for the flint glasses (SF6, SF56, SF7, F7, KzF6) but decreases with H_k for the silicate crown glasses (K7, BK7, SK7, fused silica). This result shows that H_k alone does not determine SR. For example, KzF6 has about the same Knoop hardness as the other flint glasses but shows a significantly higher surface microroughness.

The surface roughness should not correlate with Knoop hardness under conditions of deterministic microgrinding for the following reason: For a fixed infeed rate, different glasses require different forces on the tool against the glass surface. Since the force varies from glass to glass, Knoop hardness can not conveniently be normalized to give dimensions of length (the dimensions of SR). This obstacle is overcome when the fracture toughness is used in conjunction with the Knoop hardness, as shown below.

Figure 66.49 shows the correlation of the measured SR with the length scale $(K_c/H_k)^2$. An essentially linear relationship between the surface microroughness and $(K_c/H_k)^2$ holds for both the flint and crown silicate glasses, as well as the lanthanum borate glass LaK10. Although not shown here, the correlation previously shown to hold for loose-abrasive grinding,[31] namely that SR $\sim E^{1/2}/H$, does not correlate with our experimental data. The reason, of course, is that under conditions of deterministic microgrinding, the material-removal rate, rather than the nominal pressure, is held constant as in loose-abrasive grinding.

The length scale $(K_c/H_k)^2$ may be referred to as a ductility index Ξ (with units of length),

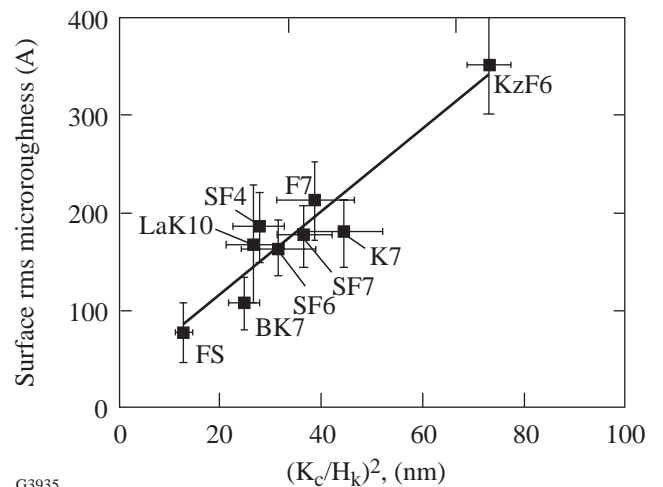$$\Xi = \left(\frac{K_c}{H_k}\right)^2, \qquad (5)$$

G3934

G3935

Figure 66.48
Correlation of measured surface roughness (with Zygo Maxim interferometer) with the Knoop hardness published in the Schott glass catalog. For flint silicate glasses SR increases with H_k, while it decreases for the crown silicate optical glasses.

Figure 66.49
Correlation of measured surface roughness (with Zygo Maxim interferometer) with the ductility index $\Xi = \left(K_c/H_k\right)^2$ of various optical glasses. The correlation holds for both flint and crown glasses, as well as fused silica. The straight line, with slope 4.2±0.5 A/nm, has correlation $R = 0.95$.

which is in reverse analogy to the brittleness index used by Lawn *et al.*[62] In that investigation the surface energy Γ was used, but their results may be recast into a form similar to ours with the identification of Γ as the energy-release rate required for crack growth, i.e., $\Gamma = \left(1 - v^2\right) K_c^2 / E$ under plane-strain crack-growth conditions, where v is the Poisson ratio. The ductility index $(K_c/H_k)^2$ provides a useful measure of the response of various glasses; for example: although fused silica has a typical fracture toughness K_c, it has a very high hardness, a low ductility index, and a low measured surface roughness. On the other hand, KzF6 has a high fracture toughness and low hardness, leading to a high ductility index and a correspondingly high surface roughness.

The concept of quantifying the "grindability" of brittle materials in terms of a brittleness index was first introduced by Aleinikov[27] in his seminal work that defined the brittleness index as linearly related to $(\ell/D)^2$, where D is the indentation diagonal in a Vickers microindentation test and ℓ the resulting crack size. Aleinikov used a fixed indentation load of 50 gf, but it is unclear whether the crack size ℓ used is the same as that defined in this work. Crack size may be measured from the center of the indentation or the length of the crack extending beyond the corner of the indentation, i.e., $\ell = c - D/2$ in our notation. In any case, $(\ell/D)^2$ is a function of the applied load P [typically $(\ell/D)^2 \sim P^{1/3}$], which is inversely proportional to the fracture toughness K_c, and proportional to the Young's modulus E. This implies that the brittleness index defined by Aleinikov can vary depending on whether the applied load is large, rather than being a load-independent material property, such as the ductility index.

Early Russian investigations in loose-abrasive grinding show that the fracture toughness, or the crack size ℓ, must be used to characterize material removal. Aleinikov's work on lapping[27] showed that the volume removal rate was proportional to ℓ^3, whereas the subsurface damage depth (the "destroyed layer" in Aleinikov's work) was proportional to ℓ. It is interesting to note that in the work on lapping by Izumitani, the volume removal rate was proportional to ℓ^2.[34,63]

It is instructive to interpret in a different way our conclusion that the measured SR scales in direct proportion to the ductility index $(K_c/H_k)^2$. We used Hill's[58] model to extract the uniaxial yield stress σ_Y of glass (see Fig. 66.50) from the measured Vickers hardness H_v. The procedure is summarized in the Appendix. In Fig. 66.50 the extracted uniaxial yield stress σ_Y is plotted versus the measured Vickers hardness, including our

current measurements and those by Izumitani.[34] The values of the uniaxial yield stress σ_Y are also shown in Table 66.V.
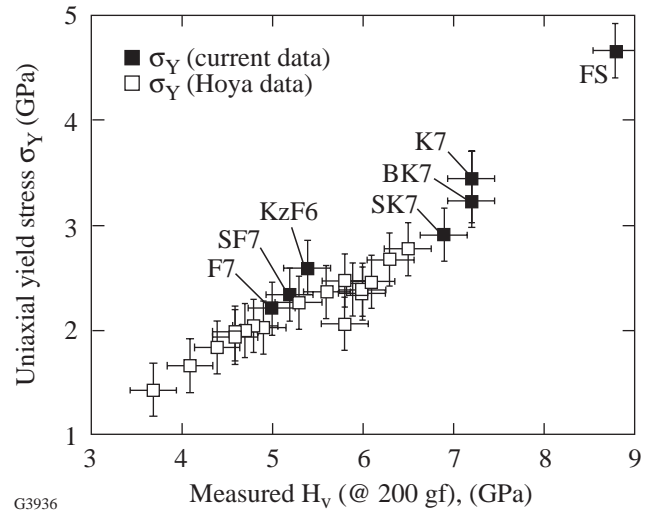

Figure 66.50
The correlation of the measured Vickers hardness (the open squares are from Izumitani[34]) with the uniaxial yield stress as calculated from the Hill analysis.[58]

The size of the plastic zone in a mode-*I* growing crack tip may be estimated from the extracted uniaxial yield stress σ_Y and the fracture toughness K_c. For an elastic, perfectly plastic material (i.e., no strain hardening), the total height of the plastic zone is[64]

$$R_p \approx 2 \, \frac{0.35}{\pi} \left(\frac{K_c}{\sigma_Y} \right)^2 . \qquad (6)$$

Figure 66.51 shows that the measured surface microroughness is about equal to the size R_p of the plastic zone. Based on this correlation, we can therefore predict the surface microroughness as

$$SR \sim R_p \approx 2 \, \frac{0.35}{\pi} \left(\frac{K_c}{\sigma_Y} \right)^2 , \qquad (7)$$

where the symbol ~ denotes "varies as." We emphasize that the numerical agreement between the extent of the plastic zone R_p and the rms surface roughness (SR) determined with the Maxim interferometer is fortuitous because the Maxim interferometer provides only a qualitative measure of the surface
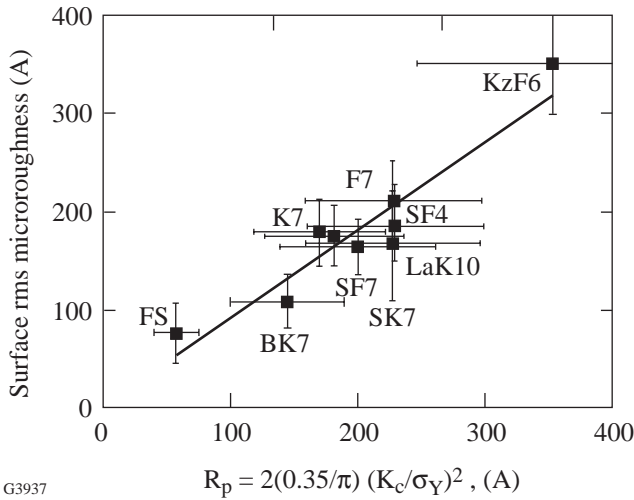
G3937

$$R_p = 2(0.35/\pi) (K_c/\sigma_Y)^2 , (A)$$

Figure 66.51
Correlation of measured surface roughness (with Zygo Maxim interferometer) with the total height R_p of the plastic zone in a crack tip growing under mode I (opening) conditions. The straight line fit has correlation $R = 0.95$.

G3938

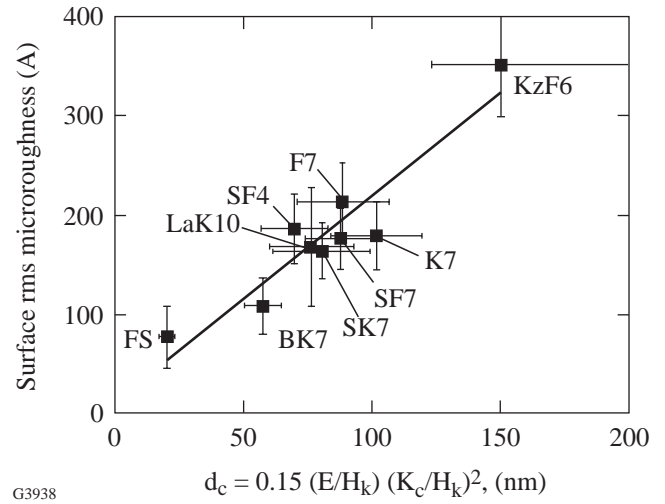$$d_c = 0.15 (E/H_k) (K_c/H_k)^2, (nm)$$

Figure 66.52
Correlation of measured surface roughness (with Zygo Maxim interferometer) with the critical depth of cut d_c, from the work of Bifano et al.[15] The straight line, with slope 2.1±0.3 A/nm, has correlation $R = 0.94$.

roughness. In any case, the size of the plastic zone at a growing crack tip is proportional to $(K_c/H_k)^2$, which was previously identified as the ductility index. The issue of the precise correlation between SR and the ductility index $(K_c/H_k)^2$ will be further examined in the next section where we discuss the surface roughness resulting from different tools.

In addition to the ductility index $(K_c/H_k)^2$ it is possible to use other material-dependent properties in correlating the surface microroughness among various glasses. Figure 66.52 shows the correlation between the measured SR and the critical depth of cut d_c, defined by Bifano et al.[15] as that material length scale distinguishing the transition from ductile- to brittle-material-removal mechanisms. It is surprising, however, that our measured SR increases with d_c. It is expected that, for a material with a low d_c, brittle removal should occur when the infeed per tool revolution exceeds d_c and, hence, yield higher surface roughness. The good correlation between SR and d_c in Fig. 66.52 may be due to the fact that the ratio E/H_k, for the materials in Figs. 66.50 and 66.51, varies only between 14 and 19 (with the exception of fused silica, for which $E/H_k = 11.1$). Thus, the correlation in Fig. 66.52 may be a result of the correlation shown in Fig. 66.49.

We have also considered the correlation between the measured surface roughness and the critical load P_c required for the formation of subsurface lateral cracks, as discussed by Chiang et al.[65,66] The correlation now becomes less effective,

which may be due to the fact that in deterministic microgrinding the infeed rate is constant, and the contact force between the tool and the glass surface spontaneously adjusts itself to accommodate the imposed material-removal rate.

Relationship to Tool Hardness
To determine whether the correlations with glass properties are retained for different tools, experiments were performed with L, N, and T hardness tools. All tools had approximately the same Young's modulus, but Vickers hardness increased approximately linearly from softer (L) to harder (T) tools. All tools had 75 concentration (18.8 vol %) of 2- to 4-μm diamonds. The glasses studied in this section included the flint glasses SF7, F7, and KzFSN5, the crown glasses K7 and SK7, as well as fused silica. The rms surface microroughness was measured with the New View 100 white light interferometer.

Figure 66.53 shows the correlation of the measured SR with the Knoop hardness for the three tools. As in Fig. 66.48, different glass groups behave differently: Surface roughness increases with hardness for the flint glasses, but decreases for the crown silicate glasses.

Figure 66.54 shows the improved correlation of the rms microroughness with the ductility index $(K_c/H_k)^2$. The ductility index can be used as a single material length scale correlating the SR with the material properties of the various glasses. This conclusion emphasizes (1) the importance of fracture and

deformation in the production of SR in deterministic microgrinding and (2) the similar behavior of various glass families (flints, crowns, fused silica). We emphasize that in loose-abrasive microgrinding (lapping), the surface microroughness is determined only by the hardness and the elastic modulus of the glass,[31] and not by the fracture toughness. That the microroughness correlates differently with the mechanical properties of glass for deterministic microgrinding and loose-abrasive microgrinding emphasizes the differences between two-body and three-body abrasive processes.
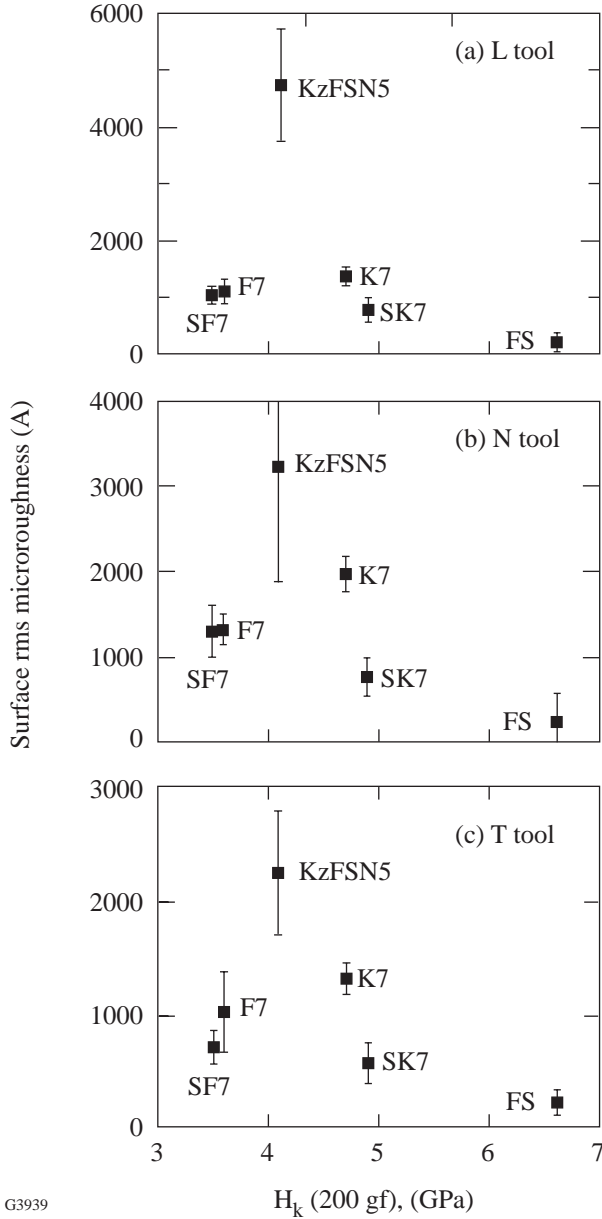
Figure 66.53
Correlation of measured surface roughness (with Zygo New View NV interferometer) with the Knoop hardness of optical glasses for (a) softer (L) tools, (b) medium (N) tools, and (c) harder (T) tools.
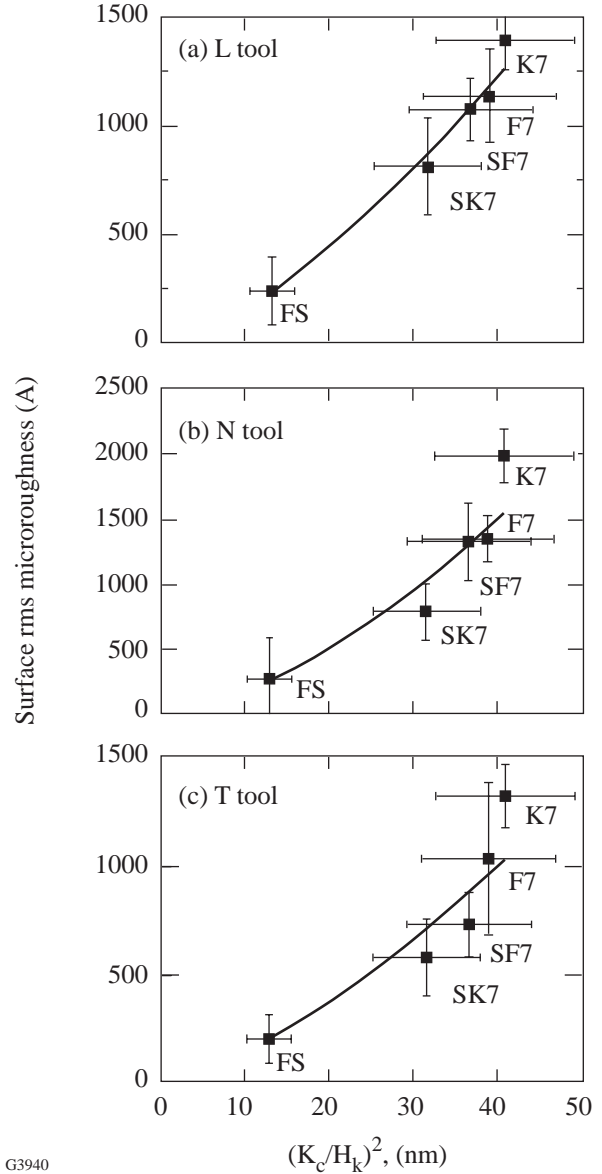
Figure 66.54
Correlation of measured surface roughness (with Zygo New View NV interferometer) with the ductility index $\Xi = \left(K_c/H_k\right)^2$ for various optical glasses for (a) softer (L) tools, (b) medium (N) tools, and (c) harder (T) tools. Power law fitting gives an exponent of 1.5 ± 0.1 for the dependence of SR on Ξ, with correlation $R = 0.92$–0.99.

The results in Fig. 66.54 [the measurement of the rms roughness by the New View 100 white-light interferometer (NV)] are consistent with the measurement of the roughness with the Maxim laser interferometer (MX), shown in Fig. 66.49. When the surface roughness of Fig. 66.54 is fitted to a power-law dependence on the ductility index $\Xi = (K_c/H_k)^2$, we find

$$\text{rms SR (NV)} \sim \Xi^m. \qquad (8)$$

The exponent $m = 1.5\pm0.1$, with confidence levels of 0.92–0.99 for the three bond hardnesses L, N, and T. On the other hand, when the surface-roughness measurements by the two different interferometers were correlated (by power-law curve fitting), we found

$$\text{rms SR (MX)} \sim \left[\text{rms SR (NV)}\right]^n, \qquad (9)$$

where the exponent $n = 0.62\pm0.15$. The large relative error in the exponent n is due to the larger variation between the two sets of measurements for the rougher surfaces.

Combining Eqs. (8) and (9), we conclude that

$$\text{rms SR (MX)} \sim \Xi^{mn}. \qquad (10)$$

Since the product (mn) is 0.93±0.27, we conclude that Eq. (10) predicts essentially a linear dependence of the surface roughness measured with the Maxim laser interferometer and the ductility index Ξ. This result is consistent with the independently measured behavior shown in Fig. 66.49.

Conclusions

We have shown that the elastic (Young's modulus), plastic (hardness), and fracture (fracture toughness) properties of glasses must all be considered in correlating the glass mechanical properties with the surface quality resulting from deterministic microgrinding using bound-abrasive tools under specified infeed rate (or material-removal rate) and when the processing parameters (relative speed, diamond size, coolant) are constant.

The material properties can be conveniently grouped into a ductility index $\Xi = (K_c/H_k)^2$, with the units of length, and proportional to the size of the plastic zone near the crack tip of a crack growing under mode I (i.e., opening) conditions. The ductility index was shown to correlate surface roughness with glass mechanical properties across glass groups such as flint, crown silicate, and fused silica. The correlation also holds for softer, medium, or harder bond tools, or when the surface microroughness is measured by different interferometric methods. The creation of surface roughness is seen as a competition between fracture and flow processes. Low ductility, achieved by a low fracture toughness or a high hardness, results in low resulting roughness.

The correlation of the surface roughness to glass properties under deterministic microgrinding conditions is distinct from the correlation under loose-abrasive (lapping) conditions, where the surface roughness is determined by the elastic and plastic properties of glass. Such a distinction is not surprising: Deterministic microgrinding proceeds under a specified infeed rate (i.e., material-removal rate), whereas lapping is under constant nominal pressure. Furthermore, lapping is a three-body abrasive process, whereas deterministic microgrinding is primarily a two-body abrasive process (although three-body abrasion can occur when a previously bound diamond abrasive grain is separated from the retaining bond matrix).

We have shown that the fracture toughness of optical glasses can be conveniently measured using Vickers microindentation. Such measurement of the near-surface glass mechanical properties is advantageous in that many measurements can be done on a single specimen. However, for glasses that show densification, such as fused silica, microindentation provides an overestimate of the fracture toughness. For glasses that deform by flow, as do most optical glasses containing network modifiers, microindentation fracture-toughness measurements are in good agreement with the fracture toughness measured by bulk methods.

We have assumed that the mechanical response of glasses may be described in terms of four fundamental properties: the elastic Young's modulus E, the Poisson ratio ν, the plastic hardness H (Vickers H_v or Knoop H_k), and the fracture toughness K_c. This set of properties may be incomplete. Future work should consider the following: hardening effects describing the increase of the flow stress with continuing deformation, effects correlating the rate of subcritical crack growth to applied loads or stress-intensity factors,[44,51,64] any chemomechanical effects on the glass properties, such as the effect of slurry chemistry,[17] or the possibility that the glass mechanical properties at very small depths (say, less than 0.1 μm) may be different from the measured properties either at deeper penetrations or by bulk methods. Of course, characterization at such low depths requires sophisticated experi-

mental techniques, such as nanoindentation. Also, subcritical crack growth is very sensitive to the chemical environment within which crack growth occurs. We are currently investigating the effects of various coolants on various glass mechanical properties.

This article concentrates on correlating the glass mechanical properties with surface features such as microroughness and subsurface damage for a variety of optical glasses, all finished under the same deterministic microgrinding process parameters. Of course, from the optics manufacturing perspective, an important complementary issue is the combination of process parameters, such as infeed rate, tool relative speed, coolant, etc., which, for a given optical glass, may be used to predict the resulting surface microroughness or other surface features. We are investigating the construction of optics manufacturing maps for deterministic microgrinding processes and are hopeful these will allow the accurate prediction of the surface features resulting from a given combination of process parameters and material properties.

ACKNOWLEDGMENT

Appendix: Hill's Extraction of Uniaxial Yield Stress from the Hardness

The model of Hill[58] examines a spherical cavity in an infinite solid. The cavity, originally of vanishing radius, is under internal pressure p, so that its current radius is a. The boundary between the plastic and elastic zones is at $r = b$, r being the spherical distance from the cavity center. The material outside the cavity is elastic, perfectly plastic with Young's modulus E, Poisson ratio v, and uniaxial stress (in tension or compression) σ_Y.

The requirement of equilibrium and radial traction continuity across the elastic-plastic boundary $r = b$ yields

$$p = \frac{2}{3}\left[1 + 3\ln\left(\frac{b}{a}\right)\right]\sigma_Y. \qquad (A\text{-}1)$$

Calculation of the elastic strains allows the determination of the (finite) radial displacements, yielding

$$\left(\frac{b}{a}\right)^3 = \frac{E}{3(1-v)\sigma_Y}. \qquad (A\text{-}2)$$

In the Hill model of indentation Vickers hardness, the pressure p required to produce the radius a is identified with the average pressure under the indenter, i.e., the hardness. Thus

$$p \to H_v. \qquad (A\text{-}3)$$

Equations (A-1)–(A-3) and elimination of the ratio b/a allow the correlation of the Vickers hardness H_v and the uniaxial yield stress σ_Y, which is found from solving the transcendental equation

$$\frac{(E/H_v)}{3(1-v)}\frac{1}{\left(\frac{\sigma_Y}{H_v}\right)} = \exp\left[-1 + \frac{3/2}{\left(\frac{\sigma_Y}{H_v}\right)}\right] \qquad (A\text{-}4)$$

for the ratio σ_Y/H_v, in terms of measurable mechanical properties such as the Young's modulus, the Vickers microhardness, and the Poisson ratio.

REFERENCES

1. H. M. Pollicove and D. T. Moore, Laser Focus World, March 1991, 145.

2. H. M. Pollicove and D. T. Moore, in *Optical Fabrication and Testing Workshop Topical Meeting*, 1992 Technical Digest Series (Optical Society of America, Washington, DC, 1992), Vol. 24, pp. 44–47.

3. D. Golini and W. Czajkowski, Laser Focus World, July 1992, 146.

4. D. Golini, A. Lindquist, M. Atwood, and C. Ferreira, in *Optical Fabrication and Testing Workshop*, 1994 Technical Digest Series (Optical Society of America, Washington, DC, 1994), Vol. 13, pp. 28–31.

5. H. Pollicove, D. Golini, and J. Ruckman, Opt. Photonics News, June 1994, 15.

6. J. Liedes, in *Current Developments in Optical Design and Optical Engineering II*, edited by R. E. Fischer and W. J. Smith (SPIE, Bellingham, WA, 1992), Vol. 1752, pp. 153–157.

7. J. C. Lambropoulos, P. D. Funkenbusch, D. J. Quesnel, S. M. Gracewski, and R. F. Gans, in *Proceedings of the Ninth Annual Meeting of the American Society for Precision Engineering* (American Society for Precision Engineering, Raleigh, NC, 1994), pp. 370–373.

8. J. C. Lambropoulos, in *Proceedings of the Ninth Annual Meeting of the American Society for Precision Engineering* (American Society for Precision Engineering, Raleigh, NC, 1994), pp. 97–100.

9. G. S. Khodakov and Yu. A. Glukhov, Sov. J. Opt. Technol. **48**, 428 (1981).

10. P. D. Funkenbusch and S. M. Gracewski, in *Optifab '94 Conference Proceedings* (sponsored by the Industrial Diamond Association of America and the Center for Optics Manufacturing, Rochester, NY, 1994).

11. P. D. Funkenbusch, Y. Y. Zhou, T. Takahashi, D. J. Quesnel, and J. Lambropoulos, in *International Conference on Optical Fabrication and Testing*, edited by T. Kasai (SPIE, Bellingham, WA, 1995), Vol. 2576, pp. 46–52.

12. A. G. Evans and D. B. Marshall, in *Fundamentals of Friction and Wear of Materials*, edited by D. A. Rigney (American Society for Metals, Metals Park, OH, 1981), pp. 441–452.

13. T. S. Izumitani, *Optical Glass*, American Institute of Physics Translation Series (American Institute of Physics, New York, 1986).

14. S. Yoshida and H. Ito, Bull. Jpn. Soc. Precis. Eng. **24**, 239 (1990).

15. T. G. Bifano, T. A. Dow, and R. O. Scattergood, Trans. ASME, B, J. Eng. Ind. **113**, 184 (1991).

16. D. Golini and S. D. Jacobs, in *Advanced Optical Manufacturing and Testing*, edited by L. R. Baker, P. B. Reid, and G. M. Sanger (SPIE, Bellingham, WA, 1990), Vol. 1333, pp. 80–91.

17. D. Golini and S. D. Jacobs, Appl. Opt. **30**, 2761 (1991).

18. Y. Namba and M. Abe, CIRP Ann. **42**, 417 (1993).

19. M. G. Schinker, Prec. Eng. **13**, 208 (1991).

20. N. J. Brown and B. A. Fuchs, in *Optical Fabrication and Testing,* 1988 Technical Digest Series (Optical Society of America, Washington, DC, 1988), Vol. 13, pp. 23–26.

21. N. J. Brown and B. A. Fuchs, in the *Proceedings of the 43rd Annual Symposium on Frequency Control* (IEEE, Piscataway, NJ, 1989), pp. 606–610.

22. J. C. Lambropoulos, T. Fang, A. Lindquist, and D. Golini, presented at the International Symposium on Manufacturing Practices and Technology, 1995 Fall Meeting of the Glass and Optical Materials Division of the American Ceramic Society, New Orleans, LA, 5–8 November 1995; also to be published in Ceramic Transactions.

23. N. J. Brown *et al.*, in the *Proceedings of the 43rd Annual Symposium on Frequency Control* (IEEE, Piscataway, NJ, 1989), pp. 611–616.

24. O. Podzimek, CIRP Ann. **35**, 397 (1986).

25. O. Podzimek, Technical Report WB-85-16, Twente University of Technology (1986), 112 pages.

26. O. Podzimek, in *High Power Lasers*, edited by E. W. Kreutz, A. Quenzer, and D. Schüöcker (SPIE, Bellingham, WA, 1987), Vol. 801, pp. 221–223.

27. F. K. Aleinikov, Sov. Phys. Tech. Phys. **27**, 2529 (1957).

28. G. S. Khodakov, V. P. Korovkin, and V. M. Al'tshu'ler, Sov. J. Opt. Technol. **47**, 552 (1980).

29. D. F. Edwards and P. P. Hed, Appl. Opt. **26**, 4670 (1987).

30. D. F. Edwards and P. P. Hed, Appl. Opt. **26**, 4677 (1987).

31. M. Buijs and K. Korpel-Van Houten, J. Mater. Sci. **28**, 3014 (1993).

32. A. L. Ardamatskii, Sov. J. Opt. Technol. **47**, 613 (1980).

33. H. Li and R. C. Bradt, J. Non-Cryst. Solids **146**, 197 (1992).

34. T. S. Izumitani, Hoya Technical Report HGW-O-7E, Hoya Glass Works, Ltd (20 February 1971).

35. R. F. Cook and G. M. Pharr, J. Am. Ceram. Soc. **73**, 787 (1990).

36. M. Sakai and R. C. Bradt, Int. Mater. Rev. **38**, 53 (1993).

37. A. G. Evans and E. A. Charles, J. Am. Ceram. Soc. **59**, 371 (1976).

38. A. G. Evans, in *Fracture Mechanics Applied to Brittle Materials*, edited by S. W. Freiman (American Society for Testing and Materials, Philadelphia, 1979), ASTM STP 678, Part 2, pp. 112–135.

39. B. R. Lawn, A. G. Evans, and D. B. Marshall, J. Am. Ceram. Soc. **63**, 574 (1980).

40. G. R. Anstis *et al*., J. Am. Ceram. Soc. **64**, 533 (1981)

41. J. Lankford, J. Mater. Sci. Lett. **1**, 493 (1982).

42. K. Niihara, R. Morena, and D. P. H. Hasselman, J. Mater. Sci. Lett. **1**, 13 (1982).

43. D. K. Shetty *et al*., J. Mater. Sci. **20**, 1873 (1985).

44. I. J. McColm, *Ceramic Hardness* (Plenum Press, New York, 1990).

45. R. L. K. Matsumoto, J. Am. Ceram. Soc. **70**, C-366 (1987).

46. Schott Glass Catalog, Publication 10000, Schott Glass Technologies Inc., Duryea, PA 18642 (1992).

47. M. Cumbo, The Institute of Optics, University of Rochester (May 1992) (unpublished work).

48. M. Cumbo, Ph.D. thesis, The Institute of Optics, University of Rochester, 1993.

49. I. M. Androsov, S. N. Dub, and V. P. Maslov, Sov. J. Opt. Technol. **56**, 691 (1989).

50. S. M. Wiederhorn *et al*., J. Am. Ceram. Soc. **57**, 337 (1974).

51. S. Wiederhorn and D. E. Roberts, prepared for NASA Manned Spacecraft Center, Structures and Mechanics Division, PR1-168-022, T-5330A, NBS, U.S. Department of Commerce, Report 10892 (1972).

52. R. F. Cook and B. R. Lawn, J. Am. Ceram. Soc. **66,** C-200 (1983).

53. A. Arora, D. B. Marshall, and B. R. Lawn, J. Non-Cryst. Solids **31**, 415 (1979).

54. J. D. Mackenzie, J. Am. Ceram. Soc. **46**, 461 (1963).

55. J. C. Lambropoulos, T. Fang, S. Xu, and S. M. Gracewski, in *Optical Manufacturing and Testing*, edited by V. J. Doherty and H. P. Stahl (SPIE, Bellingham, WA, 1995), Vol. 2536, pp. 275–286.

56. S. M. Wiederhorn, J. Am. Ceram. Soc. **52**, 99 (1969).

57. L. M. Barker, in *Fracture Mechanics Applied to Brittle Materials,* edited by S. W. Freiman (American Society for Testing and Materials, Philadelphia, 1979), ASTM STP 678, Part 2, pp. 73–82.

58. R. Hill, *The Mathematical Theory of Plasticity* (Clarendon Press, Oxford, 1950).

59. H. H. Karow, *Fabrication Methods for Precision Optics* (Wiley, New York, 1993).

60. A. Lindquist, S. D. Jacobs, and A. Feltz, in *Science of Optical Finishing*, 1990 Technical Digest Series (Optical Society of America, Washington, DC, 1990), Vol. 9, pp. 57–60.

61. Y. Zhou, P. D. Funkenbusch, D. J. Quesnel, D. Golini, and A. Lindquist, J. Am. Ceram. Soc. **77**, 3277 (1994).

62. B. R. Lawn, T. Jensen, and A. Arora, J. Mater. Sci. **11**, 573 (1976).

63. T. S. Izumitani and I. Suzuki, Glass Technol. **14**, 35 (1973).

64. T. L. Anderson, *Fracture Mechanics: Fundamentals and Applications*, 2nd ed. (CRC Press, Boca Raton, FL, 1995).

65. S. S. Chiang, D. B. Marshall, and A. G. Evans, J. Appl. Phys. **53**, 298 (1982).

66. S. S. Chiang, D. B. Marshall, and A. G. Evans, J. Appl. Phys. **53**, 312 (1982).